Frozen Translational and Rotational Motion of HIV TAT Peptide-modified Nanocargo on Neutral Lipid Bilayer.

ARTICLE *in* ANALYTICAL CHEMISTRY · APRIL 2013

Impact Factor: 5.64 · DOI: 10.1021/ac400503z · Source: PubMed

6 AUTHORS, INCLUDING:

Bo Chen
Hu Nan Normal University
111 PUBLICATIONS **1,988** CITATIONS
SEE PROFILE

Lehui Xiao
Hu Nan Normal University
22 PUBLICATIONS **297** CITATIONS
SEE PROFILE

analytical chemistry

Article

pubs.acs.org/ac

Frozen Translational and Rotational Motion of Human Immunodeficiency Virus Transacting Activator of Transcription Peptide-Modified Nanocargo on Neutral Lipid Bilayer

Lin Wei,[†,‡,∥] Xin Zhao,[‡,∥] Bo Chen,[‡] Hongchang Li,[‡] Lehui Xiao,*[,‡] and Edward S. Yeung*[,†,§]

[†]College of Chemistry and Chemical Engineering, College of Biology, State Key Laboratory of Chemo/Biosensing and Chemometrics, Hunan University, Changsha, 410082, People's Republic of China

[‡]Key Laboratory of Chemical Biology and Traditional Chinese Medicine Research, Ministry of Education, College of Chemistry and Chemical Engineering, Hunan Normal University, Changsha, Hunan, 410081, People's Republic of China

[§]Ames Laboratory, United States Department of Energy and Department of Chemistry, Iowa State University, Ames, Iowa, 50011, United States

Supporting Information

ABSTRACT: With time-resolved high-precision single-particle tracking methodologies, we explored the adsorption and thermal motion of transacting activator of transcription (TAT) peptide-modified nanocargo on a model lipid bilayer in the nonelectrostatic domain. We found that the lateral and rotational motion of TAT peptide-modified nanocargo could be effectively suppressed on the surface of neutral lipid membrane, a feature that cannot be explained by existing hypotheses. A semiquantitative association activation energy analysis revealed that multiple weak bonds were required for the initial adsorption process. As a result, the localized multiple TAT peptides on the surface of the nanocargo can provide a pathway for the creation of a net of peptide−lipid complexes (e.g., lipid domain). The dragging forces caused by these complexes effectively confined the thermal motion of the nanocargo on the fluid membrane that cannot be achieved by individual peptides with random spatial and conformational distributions. These interesting findings could provide insightful information for the better understanding of the intracellular internalization mechanism of TAT peptide-modified nanocargo and might shed new light on the development of highly efficient intracellular carriers for site-specific delivery of drugs and genes.

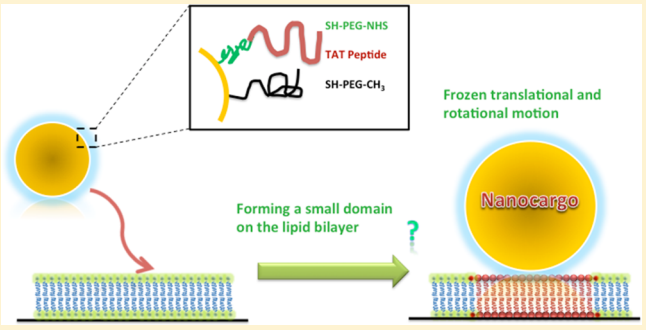

Cell-penetrating peptides have emerged as an attractive platform for intracellular delivery because they are able to translocate across the living cell membrane and carry various functional nanocargos into the cellular interior with high efficiency.[1,2] One of the best studied cell-penetrating peptides so far is the transacting activator of transcription (TAT) peptide (residues 47−57: YGRKKRRQRRR) derived from human immunodeficiency virus (HIV-1).[3,4] The HIV TAT peptide contains six arginine and two lysine residues, thus making the peptide positively charged under physiological conditions. After covalent conjugation of this cationic peptide onto the surface of nanocargo, a broad variety of functional materials including various nanoparticulate pharmaceutical carriers (liposomes, micelles, nanoparticles) can be introduced into living cells. For example, TAT peptide-modified liposomes with size as large as 250 nm still show fast and efficient gene translocation in intracranial human brain tumors.[3,5,6]

Due to the promising functionality in intracellular delivery, much attention has been paid on elucidating the detailed biophysical mechanism of the membrane translocation process.[7−12] Several lines of evidence have shown that passive electrostatic interaction plays a significant role in the process of membrane permeation.[9,13,14] Because of the electrostatic attraction between cationic amino acid residues and anionic lipids on the cell membrane, it is generally accepted that the energy barrier for the initial binding process can be effectively counteracted. However, recent single-peptide tracking results demonstrated that the electrostatic interaction alone was still not sufficient to break through the energy barrier formed by the compact lipid membrane.[10] As a consequence, additional complementary interactions are expected to be involved in the subsequent membrane translocation process. According to fluorescence and NMR spectroscopy results, the nonelectrostatic interactions (e.g., hydrogen bonds, van der Waals forces, and salt bridges) were demonstrated to contribute roughly 20% of the binding energy.[9,15] Basic understanding of the interaction mechanism between individual TAT peptides and model lipid membranes has been achieved as described above, but less is

Received: February 19, 2013
Accepted: April 13, 2013
Published: April 13, 2013

   dx.doi.org/10.1021/ac400503z | *Anal. Chem.* 2013, 85, 5169−5175

known on how TAT peptide-coated nanocargos interact with the two-dimensional fluid membrane so far. Recent studies have shown that multiple TAT peptides are commonly required on the surface of a nanocargo to facilitate highly efficient intracellular delivery.[16−18] Therefore, it is most interesting to elucidate how TAT peptide-modified nanocargos interact with the lipid membrane, especially in the nonelectrostatic domain. This is because, in a living cell system, several translocation mechanisms (endocytosis, solute carriers, channels, etc.) are commonly adopted to transport the charged objects rather than through simple passive diffusion and electrostatic association.

Herein, with time-resolved high-precision single-particle translational and rotational tracking strategies, we extensively explored the interactions between TAT peptide-modified nanocargos (with gold nanoparticle as a model system that has been widely applied in drug and gene delivery) and a neutral lipid bilayer (1-palmitoyl-2-oleoyl-*sn*-glycero-3-phosphocholine, POPC, that is naturally present in eukaryotic cell membranes and has been extensively used as model lipid membrane to study various subjects such as lipid rafts) for the first time.

EXPERIMENTAL SECTION

Chemicals and Materials. Gold nanorods with diameter 25 nm and length 70 nm were bought from Nanopartz Inc. (Loveland, CO, U.S.A.). Bis-(*p*-sulfonatophenyl)-phenylphosphine dehydrate dipotassium (BSPP), 4,7,10,13,16,19,22,25,32,35,38,41,44,47,50,53-hexadecaoxa-28,29-dithiahexapentacontanedioic acid di-*N*-succinimidyl ester (SH−PEG−NHS, $C_{46}H_{80}N_2O_{24}S_2$; MW, 1109) and *O*-[2-(3-mercaptopropionylamino)ethyl]-*O*′-methylpolyethylene glycol (SH−PEG−CH_3, $CH_3O(CH_2CH_2O)_nCH_2CH_2SH$; MW, 5000) were obtained from Sigma-Aldrich (St. Louis, MO, U.S.A.). NH_2−TAT peptide (sequence, YGRKKRRQRRR) and NH_2−TAT−FITC were purchased from AnaSpec (San Jose, CA, U.S.A.). All other chemicals were purchased from Sigma-Aldrich.

The spherical gold nanoparticles used in this experiment were synthesized by reducing $HAuCl_4$ with trisodium citrate at 110 °C.[19] In brief, 1.066 mL of 2.346×10^{-2} M $HAuCl_4$ was mixed with 98.934 mL of DI H_2O, and then the mixture was heated to 110 °C for 5 min. An amount of 10 mL of 1.455×10^{-2} M trisodium citrate was rapidly injected to the boiling solution. The mixture was vigorously stirred and refluxed for 20 min. The color of the mixture would gradually change after 5 min from colorless to pale red, pale purple, and finally to the color of wine red. After the color change process was complete, the colloidal solution was kept stirred at room temperature for another 15 min until the solution was cooled down. The size of gold nanoparticles made by this method is around 18.6 ± 1.2 nm. The larger size gold nanoparticles (40.0 ± 2.4 and 60 ± 2.5 nm) were made based on the seed-mediated growth method. Typically, for the fabrication of 40 nm gold nanoparticles, 10 mL of the seed gold nanoparticle solution was diluted to 120 mL with the final trisodium citrate concentration of 3.74×10^{-3} M. The mixture was then heated to 110 °C and followed by gradually adding 10 mL (or 24 mL for the 60 nm gold nanoparticles) of 2.346×10^{-3} M $HAuCl_4$ to the hot solution. After the reaction was complete (around 25 min), the solution was gradually cooled down to room temperature and stored at 4 °C before usage. The size of these gold nanoparticles was characterized by transmission electron microscopy (TEM) (JEM 1230, JEOL, Japan), Figure S1, Supporting Information.

Modification of TAT Peptides on the Surface of Gold Nanocargos and Density Quantification. The conjugation protocol for TAT peptides is similar to the previous procedures.[20] Briefly, 2 mL of gold nanoparticle stock solution was centrifuged at 6000 rpm for 10 min to remove the extra chemicals in the solution. The pellet was dispersed in 150 μL of 1 mg/mL BSPP solution. To graft the NHS linker onto the surface of the nanocargo, 40 μL of borate buffer (50 mM, pH 8.2) and 1.2 μL of SH−PEG−NHS (20 mM) were mixed together and then added to the purified gold nanocargo solution with gentle shaking for 3 h. After that, 0.8 μg of TAT peptides (0.2 mg/mL) was introduced to the nanocargo solution and left to react for additional 3 h. In order to increase the stability of the nanocargo in salt solution, 5 μL of 20 mM SH−PEG−CH_3 was added to the mixture and kept stirred for another 5−8 h. Those unreacted chemicals were removed by centrifugation for three times. The TAT peptide-modified gold nanocargos were suspended in 200 μL of deionized water and stored at 4 °C prior to usage.

The UV−vis spectrum and ζ-potential were adopted to verify the peptide modification process. Since the resonant scattering condition of the plasmonic nanoparticles is very sensitive to the dielectric constant of the environment close to the nanoparticle, the UV−vis absorption spectrum can then be utilized to confirm the modification process. Generally, increasing the dielectric constant close to the surface of the nanoparticle will result in noticeable red shift of the resonant scattering spectrum. As a result, given the surface of the nanocargo was successfully coated with additional layer of peptides, the UV−vis spectrum will be red-shifted. As demonstrated in Supporting Information Figure S2, there is 4 nm red shift in the resonant peak after the modification process, indicative of the successful conjugation of TAT peptides on the surface of the nanocargo. In addition, comparing the UV−vis spectrum of gold nanoparticles before and after coating with TAT, the shape of the surface plasmon resonant band is symmetrical and the bandwidth remains almost identical to that of bare gold nanoparticles. This indicates that no aggregates were formed during the surface coating process. In addition to bulk solution estimation, statistical single-particle scattering intensity analysis was applied to estimate the homogeneity of the TAT peptide-modified gold nanoparticle. As shown in Supporting Information Figure S3, the similar intensity distribution from individual particles as well as the identical mean scattering intensity clearly confirm that the TAT peptide-modified gold nanoparticles are monodispersed in the solution, a feature that is especially important for the following single-particle imaging experiments.

Besides the spectroscopic measurements, ζ-potential estimation (Nano-ZS90 Zetasizer, Malvern Instrument, U.K.) was further applied to verify the modification process. Because the TAT peptide contains six arginine and two lysine residues, in physiological environment, the peptide is positively charged. Provided the TAT peptides were successfully conjugated onto the surface of the gold nanocargo through the PEG linker, the ζ-potential of these particles should be less negatively charged than that without TAT peptides. As expected, the measured ζ-potential of the gold nanoparticles without TAT peptides is −32 mV which is noticeably more negative than that of TAT peptide-modified nanocargo (−20 mV). These results demonstrate that TAT peptides are successfully conjugated onto the surface of gold nanocargos by the procedures described above. The biological activity of these functionalized nanocargos was

dx.doi.org/10.1021/ac400503z | *Anal. Chem.* 2013, 85, 5169−5175

ascertained by checking their cellular translocation efficiency in comparison with those without TAT peptide modification (see Supporting Information Figure S4).

The density of TAT peptides on the surface of gold nanoparticles was quantified by the fluorescence-based assay.[21] In this assay, gold nanoparticles were modified by FITC-conjugated TAT peptides with other conditions being fixed. After the modification process, the FITC-labeled TAT peptides were stripped from the surface of gold nanoparticles by dithiothreitol (DTT, 0.1 M) in 0.5× PBS buffer. The concentration of FITC-labeled TAT peptides in the solution was estimated based on the concentration calibration curve. The concentration of gold nanoparticles was determined from the UV−vis absorbance (the molar extinction coefficients for 18, 40, and 60 nm gold nanoparticles are 7.27×10^8, 1.03×10^{10}, and 3.96×10^{10} M^{-1} cm^{-1}, respectively). Thus, the density of TAT peptide on the surface of the gold nanoparticle can be readily quantified through dividing the amount of TAT peptides by the number of gold nanoparticles in the solution. In this experiment, the density was estimated to be 0.34 ± 0.06 per nm^2.

Preparation of Lipid Bilayer. The lipid bilayer was prepared by the self-assembly of small unilamellar vesicles (SUVs) on the surface of a clean glass slide. SUVs were prepared according to the standard method reported before.[22,23] In short, lipid mixtures composed of 1-palmitoyl-2-oleoyl-*sn*-glycero-3-phosphocholine (POPC, Avanti Polar Lipids) and sulforhodamine 1,2-dihexadecanoyl-*sn*-glycero-3-phospho-ethanolamine (Texas-Red DHPE, 0.001% wt) were prepared in chloroform/methanol (1:1). Lipid film was then obtained by removing the solvent with nitrogen gas. Trace solvent was further removed by leaving the vial open in vacuum for 3 h. After that, the lipid film was swelled with PBS for 30 min and suspended by vortex. The as-prepared SUVs solution was diluted to a final concentration of 0.5 mg/mL by PBS buffer and then extruded 21 times through a porous polycarbonate membrane (0.1 μm) with a mini-extruder apparatus. The size of the final SUVs is around 100 nm based on the reported results.[22]

To prepare lipid bilayer on the glass slide surface, 30 μL of the freshly prepared SUVs solution was passed through a flow chamber (with width 4 mm and depth 0.2 mm) and incubated for 20−30 min. Excess vesicles were removed by washing the channel with PBS buffer extensively. Before each single-particle imaging experiment, the fluidity and integrity of the lipid bilayer were examined. Since the POPC lipid membrane was homogeneously intercalated with 0.001% of Texas-Red-labeled DHPE lipids, the integrity of the membrane could then be readily verified in the fluorescent mode. Only those membranes with well-defined integrity were further adopted for the subsequent single-particle imaging experiments. Fluorescent recovery after photobleaching (FRAP) analysis also shows that the POPC lipid molecules on the membrane are in a liquid state, Supporting Information Figure S5.

Experimental Setup for Single-Particle Optical Imaging. The single-particle imaging experiments were performed on a home-built prism-type total internal reflection scattering (TIRS) imaging microscope.[24,25] The focused excitation light from a 532 nm diode laser was reflected to the side wall of an isosceles triangle prism (IB-21.6-60.6-SF10, $25 \times 25 \times 25$ mm^3, CVI Melles Griot, U.S.A.). In order to selectively record the nanoparticle close to the lipid membrane, the entrance angle of the laser line on the glass/water interface was carefully adjusted to the value (around 75°) a little bit larger than the critical angle of 62°. A 40× objective (N.A. 0.75, Plan Apochromat, Nikon, Japan) was then used to collect the resonant scattering light from gold nanoparticles. The translational diffusion trajectories and binding kinetics of gold nanoparticles on the lipid membrane were recorded by an EMCCD (Evolve 512, Photometrics, U.S.A.) with frame rate of 28 Hz. To check the integrity of the lipid membrane, a band-pass filter (FF01-628/32-25, Semrock Inc., New York, U.S.A.) was inserted to the emission light path to block the scattered light from the laser. For single-particle rotational tracking, a half-wave plate was put in front of the CCD camera on a conventional dark-field microscope to obtain the angular-dependent scattering information.

For single-particle (or molecule) tracking, the higher signal-to-noise ratio (S/N) from the target objects, the better spatial localization precision will be achieved.[26−28] Due to the extraordinary resonant scattering efficiency from the plasmonic nanoparticle, the S/N of the probe is typically better than 30 in this study, which means that the spatial localization accuracy for individual particles on the lipid membrane can reach 7 nm based on the feature point tracking methodology, Supporting Information Figure S6.[26,29,30] This localization precision for gold nanoparticles is significantly better than that of fluorescent dyes or quantum dots under the same imaging conditions. It is worthwhile to note that the S/N is not limited in this case because there is neither photosaturation nor photobleaching effect from the plasmonic nanoparticles. It has been found that, with this imaging modality, the plasmonic nanoparticle with size as small as 3 nm can still be readily tracked with a localization precision much better than single dyes (data not shown).

Data Analysis. To precisely track the translational motion of TAT peptide-modified nanocargo on the lipid membrane, we adopted the feature point tracking algorithm for the automated detection and quantitative analysis of particle trajectories as recorded by the CCD camera.[29] The detailed procedure for image analysis is the same as that described before.[26,29,30] When the S/N ratio is around 30, the estimated localization accuracy can reach 7 nm, Supporting Information Figure S6. It should be noted that the localization precision can be readily improved by using a higher numerical aperture objective as well as stronger excitation intensity.

RESULTS AND DISCUSSION

Adsorption and Lateral Motion of TAT Peptide-Functionalized Gold Nanocargos on the Neutral Lipid Membrane. Figure 1 shows the adsorption kinetics of TAT

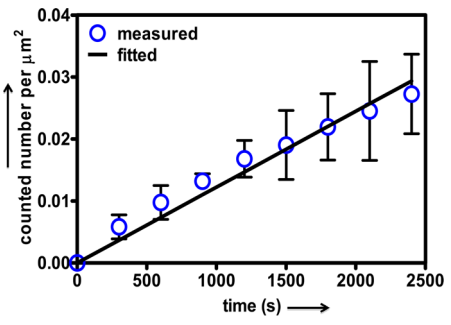

Figure 1. Binding kinetics of TAT peptide-modified nanocargos on the lipid membrane.

dx.doi.org/10.1021/ac400503z | *Anal. Chem.* 2013, 85, 5169−5175

peptide-modified 60 nm gold nanoparticles on the neutral lipid bilayer at 37 °C. The slow association rate and linear trend of the binding kinetics indicate that the effective binding probability is quite low and the adsorption/desorption equilibrium has not been reached during the time window of observation. From the real-time single-particle tracking results, we found that the majority of nanoparticles underwent semielastic collisions on the neutral lipid bilayer. The sticking time of those collision events was too short to be discriminated by our CCD camera with a temporal resolution of 28 Hz, which indicates that no stable bonds were formed from those semielastic collisions. Occasionally, the collisions were followed by effective association on the membrane. In contrast to the high frequency of collision, the low sticking probability shows that the adsorption process is kinetically controlled. Close inspection of the time-resolved diffusion trajectories led to the interesting observation that, once an effective association has taken place, the lateral motion of the nanocargo was nearly frozen on the membrane. No evidence of translational motion in the tens of nanometers range (tracked by point-spread-function localization) was found (Figure 2a). In order to assess

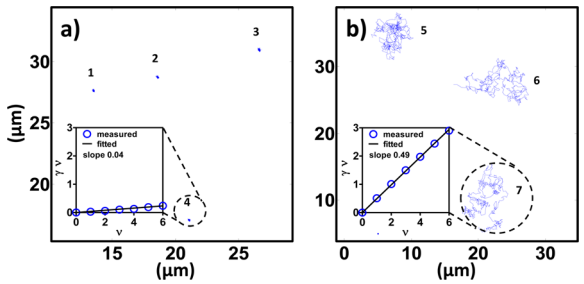

Figure 2. Diffusion mode analyses of gold nanoparticles on the lipid membrane. Representative trajectories of TAT peptide-modified (a) and PEG-modified (b) nanocargos on the lipid bilayer with the tracking time of 18 s. The moment scaling spectra for tracks 4 and 7 are shown in the subplot of panels a and b, respectively.

the detailed motion of these nanocargos other than by visual inspection, we classified their diffusion modes with the slope of moment scaling spectrum, S_{MSS}.[26,31,32] Briefly, for strongly self-similar processes, the moment scaling spectrum shows a straight line through the origin. The random diffusion mode has a slope of moment scaling spectrum of 0.5. When the motion is confined (subdiffusion), S_{MSS} will fall into the region between 0 and 0.5. For directed movement, S_{MSS} falls into the region between 0.5 and 1. The subplot in Figure 2a shows the representative S_{MSS} plot for track 4. Notably, the value of S_{MSS} is far smaller than 0.5, indicative of strongly confined diffusion. It is worth to note that this restriction effect is not a rare event; more than 96% of nanocargos (from 62 samples) exhibit S_{MSS} values much smaller than 0.5.

The high-precision single-particle localization analyses further revealed that the apparent two-dimensional (2D) diffusion constant of those adsorbed nanoparticles was only $(8.5 \pm 2.4) \times 10^{-3}$ $\mu m^2/s$. This value is around 2 orders of magnitude smaller than the theoretical value of 0.4 $\mu m^2/s$ on the lipid membrane determined by the Saffman−Delbruck model, where the hydrodynamic dragging forces caused by lipid molecules are corrected.[33] The poor agreement between these two values directly shows that the interaction between the TAT peptide-modified nanocargo and the neutral lipid bilayer cannot be simply explained by the classical hydrodynamic mechanism. This argument is verified by a control experiment in which TAT peptides were replaced by PEG molecules. Since the PEG molecule does not contain amine or carboxyl groups as the TAT peptide, the interaction between the PEG-modified gold nanoparticles and the POPC lipid bilayer can be approximated by the classical hydrodynamic interaction regime. In other words, the PEG-loaded nanocargos would "float" on the surface of the membrane and show noticeable translational movement once they were trapped on the lipid bilayer. As expected, apparent lateral diffusion for these control particles on the 2D fluid membrane was readily observed (Figure 2b). The measured 2D diffusion constant (1.1 ± 0.2 $\mu m^2/s$) was very close to the theoretical value. In agreement with the diffusion coefficient estimates, the diffusion mode classification also revealed remarkably different diffusion behavior for the PEG-modified nanocargos (random diffusion mode) in contrast to that of TAT peptide-modified nanocargo (Figure 2b).

From the previous single-peptide tracking experiments on an artificial lipid bilayer, the trapped (individual) TAT peptides were found to be solely floating on the surface of the lipid membrane regardless of the charge state of the matrix.[10] The lateral diffusion coefficient of the single peptide was not influenced by the phase state of lipids or the concentration of TAT peptide on the membrane. Even on an anionic lipid membrane, the TAT peptide still showed similar diffusion behavior (with an only slightly decreased diffusion coefficient of 3.3 ± 0.2 $\mu m^2/s$, in comparison with the value of 5.3 ± 0.2 $\mu m^2/s$ on the neutral surface). Those results provide a strong argument that individual TAT peptides cannot overcome the energy barrier required to penetrate the membrane through pure electrostatic association and also do not form agglomerates (or "carpet") on the surface even at a concentration as high as 2 μM. This behavior is noticeably different from that of antimicrobial peptides (a positively charged cell penetration peptide), where small aggregates can be formed on the membrane by passive diffusion. These will gradually break the integrity of the lipid bilayer into small pores by either barrel−stave or carpet mode.[34] If such processes also applied to the case of TAT peptide-modified nanocargo, we would have observed analogous lateral diffusion behavior from those trapped nanocargos on the fluid membrane. The inconsistency in the diffusion mode in these two cases indicates that the localized multiple TAT peptides do not behave independently once they are localized in the nanodomain.

Activation Energy Estimation for the Adsorption Process. To obtain in-depth insights into the interaction mechanism between the TAT peptide-modified nanocargo and the lipid bilayer, we determined the activation energy of the association process based on the classical collision theory.[35,36] Without loss of generality, we simplified the binding process into a second-order ligand/receptor association process. The increasing number of nanocargos on the lipid surface as a function of time can then be described as $dN/dt = k_a C_s C_n$, where k_a is the association constant, C_s is the concentration of the available binding sites on the lipid bilayer, and C_n is the concentration of the nanoparticles in the flow channel (10 pM). Ideally, the available binding sites on the lipid bilayer within 1 μm^2 for 60 nm gold nanoparticles would be on the order of 10^2, which is significantly larger than the number of the adsorbed gold nanoparticles on the lipid surface. Moreover, because the number of effectively adsorbed nanoparticles on the surface of the lipid bilayer is also much smaller than that in the bulk solution (Figure 1), the above association equation should

dx.doi.org/10.1021/ac400503z | Anal. Chem. 2013, 85, 5169−5175

show a linear trend in the early stage due to the semiconstant concentration of the reactant. Through fitting the kinetic adsorption curve with the equation described above, the calculated association constant is $\sim 1 \times 10^3$ M^{-1} s^{-1}.

On the basis of the collision theory, the activation energy of E_a for the association process can be represented as $E_a = [\ln(Q) - \ln(k_a)]k_BT$, where Q is the diffusion collision frequency factor, k_B is the Boltzmann constant, and T is the absolute temperature. For a two-dimensional diffusion reaction between a spherical particle and an immobilized binding site on a surface, the frequency factor can be approximated as $Q \approx 2000\pi RDN_a$, where R is the radius of the contact sphere (30 nm), D is the diffusion constant of the particle in solution, and N_a is Avogadro's number.[36] Introducing the diffusion coefficient (8.2 $\mu m^2/s$, determined by the Stokes–Einstein law) of 60 nm gold nanosphere in bulk solution to the above equation, the activation energy was estimated to be 0.35 eV, which is around 3 times larger than a typical weak bond, e.g., hydrogen bond. The above semiquantitative estimate clearly illustrates that several synchronized weak bonds are required for the initial effective association process to compensate for the energy barrier. This process is kinetically limited and explains the low adsorption probability for the collision process on the neutral lipid surface ($\sim 1.3 \times 10^{-6}$). However, the remaining question why the lateral motion of TAT peptide-modified nanocargo is drastically suppressed on the neutral lipid membrane still needs to be clarified.

Rotational Dynamics of TAT Peptide-Functionalized Gold Nanocargos on the Neutral Lipid Membrane. As reported before, several lines of evidence have demonstrated that the locally concentrated antimicrobial peptides can generate small pores on the lipid membrane.[34] If the concentrated TAT peptides on the surface of the nanocargo possess comparable functionality, the lateral motion of the nanocargo might be inhibited on the surface of lipid bilayer. However, the rotational dynamics of an anisotropic nanocargo will not be significantly suppressed due to the lack of anchoring sites on the side wall. To comprehend the above scenario, we used TAT peptide-modified gold nanorod (with the same modification strategy) as a robust and sensitive rotational sensor to explore the local order of the lipid bilayer.

It has been shown that the resonant scattering of light from single gold nanorods can be reasonably approximated as the oscillations from three perpendicular dipoles with directions along three principal axes, respectively, i.e., transverse and longitudinal oscillations.[37] In this work, we derived the rotational dynamics of individual gold nanorods through selectively exciting the nanorod in the longitudinal mode. The angle-dependent polarized scattering signal was then discriminated by placing a half-wave plate in the emission light path. The quantitative relationship between the orientation angle and scattering signal can be described as $\Phi = \arccos([I_p/(I_m\sigma)]^{1/2})$, where Φ is the in-plane azimuthal angle, I_p is the polarizer modulated scattering signal from the gold nanorod, I_m is the intensity of the scattering signal from the same gold nanorod without the wave plate, and σ is the transmission efficiency of the wave plate.

If the concentrated TAT peptides on the surface could facilitate the nanocargo to break into or form small pores on the lipid bilayer, we could then expect either randomly oriented gold nanorods dispersed on the lipid bilayer in three-dimensional (3D) or random rotational motion from them regardless of the confined lateral motion as discussed above. Interestingly, we found that all of the gold nanorods on the lipid bilayer were lying in an in-plane mode (which was characterized by the defocused imaging method[37]), accompanied by frozen lateral motion again. In the control experiment, we did not observe any noticeable adsorption from TAT peptide-modified nanorods on a bare glass slide surface. Thus, the rotational limiting effect due to the defects on the lipid membrane can be reasonably neglected. The time-resolved in-plane angular variations from 90% of gold nanorods (56 samples) on the lipid membrane were less than 10° within 18 s. Four representative tracks are shown in Figure 3. The

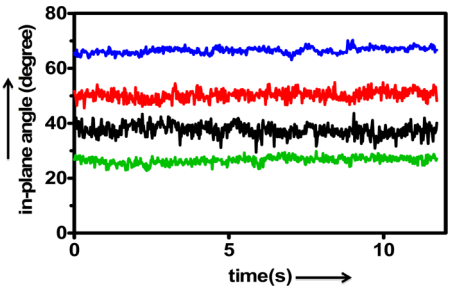

Figure 3. Time-dependent in-plane angular rotational dynamics of four TAT peptide-modified gold nanorods on the lipid membrane.

rotational velocity of these nanorods was found to be even slower than that of the nanorod confined on the lipid bilayer through limited number of biotin/streptavidin interactions on the side wall (~ 0.025 s^{-1}).[23] These interesting results imply that the hypothesis of spatial confinement effect through the formation of lipid pores on the lipid membrane is not sufficient to cause the simultaneously confined lateral and rotational motions for the nanorod.

On the basis of the above results, it is reasonable to propose that the inhibited lateral and rotational motion of TAT peptide-modified nanocargo on the neutral lipid bilayer can be ascribed to the dragging forces resulted from a net of peptide–lipid complexes, Scheme 1. Once an initial effective sticking event started, the barrier (activation energy) for the remaining neighboring TAT peptides would be reduced because of the locally enhanced reaction probability and reduced thermal motion. As a consequence, this collective effect can facilitate the formation of other multiple bonds in the local area which will create a confined lipid domain around the surface of the nanocargo.[22,38,39] The dragging force caused by the lipid domain can not only inhibit the translational motion of the nanocargo but also freeze their rotational motion.[22,23,39] Meanwhile, this binding process will lead to an increased local lipid order; that is, the synchronized TAT peptides on the nanocargo surface could significantly confine the thermal motion of lipid molecules on the sticking site. These arguments are well in accordance with previous experimental results where the formation of small domains by multiple bonds between biomolecules on the model lipid bilayer could remarkably inhibit the translational or rotational motion of a nanoparticle on the lipid membrane.[22,23,38,39] Analogous confinement effects were also observed recently in the case of protein-modified nanocargo on a living cell membrane.[26]

The current experimental results also indicate that the formation of small domains would be a promoting process for TAT peptide-mediated intracellular translocation, because the small domain can effectively reduce the lateral and rotational

dx.doi.org/10.1021/ac400503z | Anal. Chem. 2013, 85, 5169–5175

Scheme 1

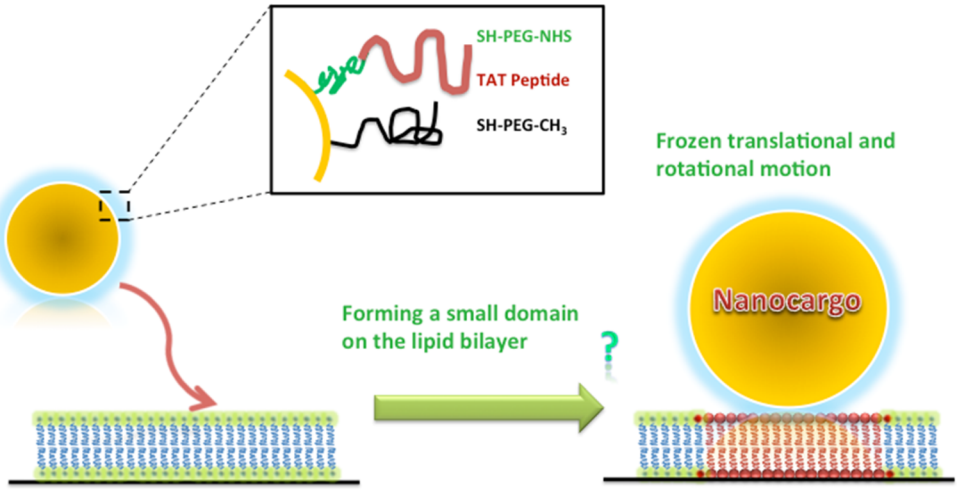

diffusions of the trapped nanocargo on the cell membrane and to some extent can facilitate the negative curvature formation for the concomitant intracellular translocation process. Additional studies also show that this confinement effect is not size-dependent (data not shown). Smaller size gold nanoparticles with diameters of 18 and 40 nm also exhibited similar restriction effects on the neutral lipid bilayer, indicative of the universal biological functionality of TAT peptide as a highly efficient intracellular translocation platform.

CONCLUSION

In summary, with the TIRS imaging strategy, the interaction between a TAT peptide-modified gold nanoparticle and neutral lipid bilayer was extensively explored for the first time. The above findings at the single-particle level on the model lipid membrane provide complementary insight into the intracellular uptake mechanism of TAT peptide-modified nanocargo in living cell systems. Moreover, the single-particle imaging methodology presented here demonstrates a robust platform to extensively explore interface interactions in general with high spatial and temporal resolutions.

ASSOCIATED CONTENT

Supporting Information

Additional information as noted in text. This material is available free of charge via the Internet at http://pubs.acs.org.

AUTHOR INFORMATION

Corresponding Author

*E-mail: lehuixiao@gmail.com (L.X.); yeung@ameslab.gov(E.S.Y.).

Author Contributions

‖The first two authors contributed equally to this work.

Notes

The authors declare no competing financial interest.

ACKNOWLEDGMENTS

This work was partially supported by NSFC 21205037 and the aid program for science and technology innovation research team in higher education institutions of Hunan Province (2010TT1001). E.S.Y. was supported by the U.S. Department of Energy, Office of Basic Energy Sciences, Division of Chemical Sciences, Geosciences, and Biosciences through the Ames Laboratory. The Ames Laboratory is operated for the U.S. Department of Energy by Iowa State University under contract no. DEAC02-07CH11358. L.W. expresses thanks for the partial financial support from the program of China Scholarships Council. B.C. thanks the partial support from the National "863" Research Foundation (2010AA023001), the NSFC (20927005, 21275049).

REFERENCES

(1) Zorko, M.; Langel, U. *Adv. Drug Delivery Rev.* **2005**, *57*, 529−545.
(2) Fonseca, S. B.; Pereira, M. P.; Kelley, S. O. *Adv. Drug Delivery Rev.* **2009**, *61*, 953−964.
(3) Torchilin, V. P. *Adv. Drug Delivery Rev.* **2008**, *60*, 548−558.
(4) Brooks, H.; Lebleu, B.; Vives, E. *Adv. Drug Delivery Rev.* **2005**, *57*, 559−577.
(5) Gupta, B.; Levchenko, T. S.; Torchilin, V. P. *Oncol. Res.* **2007**, *16*, 351−359.
(6) Torchilin, V. P.; Rammohan, R.; Weissig, V.; Levchenko, T. S. *Proc. Natl. Acad. Sci. U.S.A.* **2001**, *98*, 8786−8791.
(7) Ciobanasu, C.; Siebrasse, J. P.; Kubitscheck, U. *Biophys. J.* **2010**, *99*, 153−162.
(8) Mishra, A.; Lai, G. H.; Schmidt, N. W.; Sun, V. Z.; Rodriguez, A. R.; Tong, R.; Tang, L.; Cheng, J.; Deming, T. J.; Kamei, D. T.; Wong, G. C. L. *Proc. Natl. Acad. Sci. U.S.A.* **2011**, *108*, 16883−16888.
(9) Tiriveedhi, V.; Butko, P. *Biochemistry* **2007**, *46*, 3888−3895.
(10) Ciobanasu, C.; Harms, E.; Tünnemann, G.; Cardoso, M. C.; Kubitscheck, U. *Biochemistry* **2009**, *48*, 4728−4737.
(11) Mishra, A.; Gordon, V. D.; Yang, L.; Coridan, R.; Wong, G. C. L. *Angew. Chem., Int. Ed.* **2008**, *47*, 2986−2989.
(12) Ziegler, A.; Li Blatter, X.; Seelig, A.; Seelig, J. *Biochemistry* **2003**, *42*, 9185−9194.
(13) Vives, E.; Brodin, P.; Lebleu, B. *J. Biol. Chem.* **1997**, *272*, 16010−16017.
(14) Thorén, P. E. G.; Persson, D.; Isakson, P.; Goksör, M.; Onfelt, A.; Nordén, B. *Biochem. Biophys. Res. Commun.* **2003**, *307*, 100−107.
(15) Su, Y.; Waring, A. J.; Ruchala, P.; Hong, M. *Biochemistry* **2010**, *49*, 6009−6020.
(16) Yuan, H.; Fales, A. M.; Vo-Dinh, T. *J. Am. Chem. Soc.* **2012**, *134*, 11358−11361.
(17) Pan, L.; He, Q.; Liu, J.; Chen, Y.; Ma, M.; Zhang, L.; Shi, J. *J. Am. Chem. Soc.* **2012**, *134*, 5722−5725.
(18) de la Fuente, J. M.; Berry, C. C. *Bioconjugate Chem.* **2005**, *16*, 1176−1180.
(19) Xiao, L.; Zhou, R.; He, Y.; Li, Y.; Yeung, E. S. *J. Phys. Chem. C* **2009**, *113*, 1209−1216.
(20) Sun, W.; Wang, G.; Fang, N.; Yeung, E. S. *Anal. Chem.* **2009**, *81*, 9203−9208.

(21) Thaxton, C. S.; Hill, H. D.; Georganopoulou, D. G.; Stoeva, S. I.; Mirkin, C. A. *Anal. Chem.* **2005**, *77*, 8174−8178.
(22) Yang, Y.-H.; Nam, J.-M. *Anal. Chem.* **2009**, *81*, 2564−2568.
(23) Pierrat, S.; Hartinger, E.; Faiss, S.; Janshoff, A.; Sönnichsen, C. *J. Phys. Chem. C* **2009**, *113*, 11179−11183.
(24) Axelrod, D. *Traffic* **2001**, *2*, 764−774.
(25) Axelrod, D.; Burghardt, T. P.; Thompson, N. L. *Annu. Rev. Biophys. Bioeng.* **1984**, *13*, 247−268.
(26) Xiao, L.; Wei, L.; Liu, C.; He, Y.; Yeung, E. S. *Angew. Chem., Int. Ed.* **2012**, *51*, 4181−4184.
(27) Thompson, R. E.; Larson, D. R.; Webb, W. W. *Biophys. J.* **2002**, *82*, 2775−2783.
(28) Ober, R. J.; Ram, S.; Ward, E. S. *Biophys. J.* **2004**, *86*, 1185−1200.
(29) Sbalzarini, I. F.; Koumoutsakos, P. *J. Struct. Biol.* **2005**, *151*, 182−195.
(30) Xiao, L.; Qiao, Y.; He, Y.; Yeung, E. S. *J. Am. Chem. Soc.* **2011**, *133*, 10638−10645.
(31) Ferrari, R.; Manfroi, A.; Young, W. *Physica D* **2001**, *154*, 111−137.
(32) Ewers, H.; Smith, A. E.; Sbalzarini, I. F.; Lilie, H.; Koumoutsakos, P.; Helenius, A. *Proc. Natl. Acad. Sci. U.S.A.* **2005**, *102*, 15110.
(33) Saffman, P. G.; Delbrück, M. *Proc. Natl. Acad. Sci. U.S.A.* **1975**, *72*, 3111−3113.
(34) Brogden, K. A. *Nat. Rev. Microbiol.* **2005**, *3*, 238−250.
(35) Fox, C. B.; Wayment, J. R.; Myers, G. A.; Endicott, S. K.; Harris, J. M. *Anal. Chem.* **2009**, *81*, 5130−5138.
(36) Bally, M.; Gunnarsson, A.; Svensson, L.; Larson, G.; Zhdanov, V.; Höök, F. *Phys. Rev. Lett.* **2011**, *107*, 188103-1−188103-5.
(37) Xiao, L.; Qiao, Y.; He, Y.; Yeung, E. S. *Anal. Chem.* **2010**, *82*, 5268−5274.
(38) Naji, A.; Levine, A. J.; Pincus, P. A. *Biophys. J.* **2007**, *93*, L49−L51.
(39) Lee, G. M.; Ishihara, A.; Jacobson, K. A. *Proc. Natl. Acad. Sci. U.S.A.* **1991**, *88*, 6274−6278.